OPEN ACCESS

University of BRISTOL

Peer reviewed version

Link to published version (if available):
10.1016/j.conengprac.2018.08.012

Link to publication record in Explore Bristol Research

PDF-document

University of Bristol - Explore Bristol Research
General rights

An Interactive Control Architecture for Interpersonal Coordination in Mirror Game

Chao Zhai, Michael Z. Q. Chen, Francesco Alderisio, Alexei Yu. Uteshev, Mario di Bernardo [*]

August 9, 2018

Abstract

In this work, an interactive control architecture based on velocity segments is developed to generate the human-like trajectories in the mirror game, a simple yet effective paradigm for studying interpersonal coordination, and the existence of velocity segments possessing a prescribed signature is theoretically guaranteed. Then an online control algorithm for the architecture is proposed to produce joint improvised motion with a human player or another virtual player while exhibiting some desired kinematic characteristics. Finally, the transition from solo motions to joint improvised motions is illuminated, and the proposed control architecture is validated by matching the experimental data.

Keywords: Control architecture, PD control, motor signature, mirror game, virtual player.

1 Introduction

People suffering from social deficits (i.e., schizophrenia or autism) find it hard to engage in social activities and interact with others, which inevitably brings sorrow to themselves and their

[*]Chao Zhai is with Institute of Catastrophe Risk Management, Nanyang Technological University, 50 Nanyang Avenue, Singapore 639798. Michael Z. Q. Chen is with School of Automation, Nanjing University of Science and Technology, Nanjing, Jiangsu 210094, P. R. China. Francesco Alderisio and Mario di Bernardo are with Department of Engineering Mathematics, University of Bristol, Merchant Venturers' Building, Woodland Road, Bristol, BS8 1UB, United Kingdom. Mario di Bernardo is also with Department of Electrical Engineering and Information Technology, University of Naples Federico II, 80125 Naples, Italy. Alexei Yu. Uteshev is with Faculty of Applied Mathematics, St. Petersburg State University, Universitetskij pr.35, Petrodvorets, 198504, St. Petersburg, Russia. Corresponding author: Michael Z. Q. Chen (mzqchen@outlook.com). Fax: 025-84303010. Declarations of interest: none.

relatives [1, 2]. The theory of similarity in Social Psychology suggests that individuals prefer to cooperate with others sharing similar morphological and behavioral features, and that they tend to unconsciously coordinate their movements [3, 4, 5]. It has been shown that motor processes caused by interpersonal coordination are closely related to mental connectedness, and that motor coordination between two people promisingly contributes to social attachment [6, 7, 8].

The *mirror game* provides a simple paradigm to study social interactions and the onset of motor coordination among human beings, as it happens in improvisation theater, group dance and parade marching [9, 10]. In order to enhance social interaction through motor coordination, it would be desirable to create a virtual player (VP) or computer avatar capable of playing the mirror game with a human subject (typically the patient) either by mimicking similar kinematic characteristics or producing dissimilar ones [11]. Indeed, this would allow modulation of the kinematic similarity of the VP while maintaining a certain level of coordination with the human player (HP) so that the latter is unconsciously guided towards the direction of some desired movement features. Within this scope, the European Project "AlterEgo" was launched [12]. The purpose of the project is to promote social interaction of patients suffering from mental impairments (e.g., autism and schizophrenia) through motor coordination. Essentially, it aims at developing a new rehabilitation method to enhance the social competence of patients with social deficits by using virtual reality and humanoid robots.

Human-robot interaction finds extensive applications in haptic interfaces[13, 14], person recognition [15] and human mental development [16]. Specifically, [14] investigates the control of human arm movement in the cooperative welding process with the robot. [15] illustrates the emergence of person recognition through mutual imitation, whereas [16] evaluates the effects of human participants on the robot learning of social signature through an imitation game. It is demonstrated that the recognition of facial expressions and postures can be achieved via a sensory-motor architecture based on neural networks.

In this work, a customized human-like VP is created to socially interact with a HP in the mirror game. The main challenge is to develop a mathematical model capable of driving the VP or robot to joint-improvise with a HP in the mirror game, while guaranteeing an assigned *motor signature* as defined in [17, 18]. The first step towards this goal is to design a control architecture able to generate *in-silico* trajectories reproducing the motor signature exhibited by a certain HP playing solo. In so doing, an architecture based on velocity segments is proposed [18]. The second step is to provide such architecture with an online control algorithm allowing the VP to produce joint improvised motions and interact with a HP or another VP.

2

Much research effort has been spent on the design of control architectures for the virtual agent or robot [19, 20, 21, 22, 23, 24]. To be specific, [19, 20] develop a cognitive architecture of a VP in the mirror game by reconciling the movement tracking with individual motor signature in the framework of optimal control theory; [21] investigates the generation of goal-directed movements for robotic agents via behavioral dynamics in repetitive joint action tasks; [22] introduces a paradigm called *human dynamic clamp*, which enables real-time interaction between a HP and a VP driven by the model of coordination dynamics; [23] presents an adaptive control algorithm for the VP to track the human leader in the mirror game; [24] designs a coupled dynamical system for studying real time interaction between a HP and a computer avatar driven by the Haken-Kelso-Bunz (HKB) model [25].

However, in the aforementioned works the time series of a HP obtained from solo trials have to be used in order to generate the joint motion of a customized VP [19, 20, 23, 26], which limits its movement diversity due to the finite number of available pre-recorded trajectories. The proposed approach here overcomes this drawback by allowing the VP to autonomously exhibit any motor signature with specified kinematic features (characterizing the solo motion of a given HP) during the interaction with another agent. Here the main contributions of this work are listed below.

1. A novel perspective on modeling human movement and on the generation of movement trajectory of a customized VP in the mirror game is offered, which complements previous investigations [19, 20, 23, 26]. Specifically, this work is based on velocity segments characterizing the movement similarity, while previous work focused on probability density functions of velocity time series.

2. The control architecture proposed in this work is able to spontaneously generate solo movement trajectories of a given HP instead of using pre-recorded time series [19, 20, 23, 26].

3. In previous investigations, a boundary value problem had to be solved at each time step in order to generate the motion of a customized VP, which results in high computation costs [19, 20, 26]. Here, the solution to a simple differential equation allows to produce the real-time motion trajectory of a VP with relatively low computation costs.

The outline of this paper is given as follows. Section 2 introduces the experimental paradigm of the mirror game, a quantitative marker of motor signatures, and their construction method.

3

Figure 1: Mirror game set-up at the University of Montpellier [20]. Two horizontal strings are mounted perpendicularly at eye level and centrally between the two human participants. Two small balls are mounted on the parallel strings, respectively. Human participants are instructed to hold the handle beneath each ball and move it along the string back and forth. Cameras are installed around the participants to collect experimental data and record their movement trajectories. In solo trials, only one human participant is instructed to perform the motion. In joint trials, two human participants are seated opposite each other and interact while moving their respective ball.

Section 3 focuses on the design of a control architecture for the VP. Specifically, an algorithm capable of generating solo motions with prescribed kinematic features is developed, followed by an online control algorithm allowing the VP to produce joint improvised motion with another agent. Experimental validations are carried out in Section 4 to validate the proposed approach. Finally, Section 5 makes a conclusion and discusses future directions.

2 Preliminaries

2.1 Mirror game

The mirror game is a simple yet effective paradigm to investigate the onset of social motor coordination between two players and describe their movement imitation at high temporal and spatial resolution [9, 18, 27]. Figure 1 shows the experimental set-up of mirror game to collect the experimental data, which are used to validate the proposed numerical algorithms.

The mirror game can be played in three different experimental conditions [17]:

1. Solo Condition: This is an individual trial. Participants perform the game on their own

4

and try to create interesting motions.

2. Leader-Follower Condition: This is a collaborative round, whose purpose is for the participants to create synchronized motions. One player leads the game, while the other tries to follow the leader's movement.

3. Joint-Improvisation Condition: Two players are required to imitate each other, create synchronized and interesting motions and enjoy playing together, without any designation of leader and follower roles.

Human movements in solo condition reflect their intrinsic dynamics, i.e., their individual motor signature [17]. On the other hand, participants reconcile their respective intrinsic dynamics with the communal goal (movement synchronization) in leader-follower or joint-improvisation condition. Here, the focus is on the mathematical modeling of human coordination in solo and joint improvisation (JI) condition, and light is shed on their interconnection.

2.2 Motor signature

In the mirror game, motor signatures refer to the unique, time-persistent, kinematic self-similarity characteristics of human hand movements in solo condition [17, 18, 28]. They allow to quantify the kinematic similarity between agents [17], distinguish patients from healthy human participants, as well as assess the effect of interpersonal coordination on patients' behavior in joint action tasks [29]. It has been shown that a possible candidate of motor signature is the probability density function (PDF) of velocity time series in solo trials [17, 28]. The PDF of velocity time series is used to quantify the probability of the velocity falling within a particular range of values. This probability is given by the integral of the above PDF of velocity time series over the given range. As a consequence, a control architecture based on pre-recorded HP velocity profiles was developed for the VP to achieve real-time interaction in leader-follower and joint-improvisation conditions [19, 20, 23].

Notably, skewness and kurtosis of normalized velocity segments provide also a suitable complement as a marker of motor signature [18]. Specifically, velocity segments can be obtained by partitioning the time series of velocity through time points of zero velocity (see segments in the red dash boxes in the time-velocity plane of Fig. 2). The *original* velocity segment is described by the period and portion of velocity time series between two consecutive points of zero velocity (see Fig. 3(a)). The original velocity segment is then normalized over the time interval $[0, 1]$ (see Fig. 3(b)) and divided by the area between the segment curve and the time axis. In so
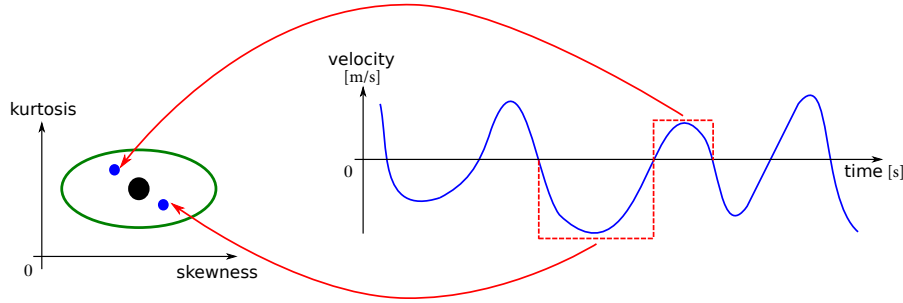
5

Figure 2: Motor signature of a human participant based on velocity segments in the mirror game [18]. The blue curve denotes the velocity time series of a human participant in a solo trial. The velocity segments in the red dashed boxes are normalized and then mapped as two blue points in the skewness-kurtosis (S-K) plane. Solo motions of a human participant in the S-K plane correspond then to a green ellipse, whose center is individuated by a black circle, which contains the majority of mapped segments.

doing, the *normalized* (or *base*) segment of velocity is obtained (see Fig. 3(c)). The normalized velocity segment allows to compute its skewness and kurtosis [18].

The green ellipse in Fig. 2 gives a graphical representation of velocity-segments-based individual motor signatures, represented by:

$$\frac{(z_s - \mu_s)^2}{\sigma_s^2} + \frac{(z_k - \mu_k)^2}{\sigma_k^2} = 1 \tag{1}$$

where z_s and z_k represent the horizontal and vertical coordinates in the skewness-kurtosis (S-K) plane, with μ_s and μ_k (σ_s and σ_k) referring to mean values (standard deviations) of skewness and kurtosis of the normalized velocity segments, respectively.

The main goal is to develop a control architecture for the VP to produce human-like solo movements and joint improvised trajectories with the desired values for skewness and kurtosis of normalized velocity segments, such that the kinematic features of a certain HP can be reproduced without making use of limited pre-recorded trajectories.

2.3 Base segment of velocity

The aim of this section is to show how to construct base segments of velocity with specified values of skewness and kurtosis. First, the smooth point-to-point movement of human hand is described by a polynomial function with unknown coefficients. Then, a system of nonlinear equations is established to account for the constraints on skewness and kurtosis. Finally, the existence of
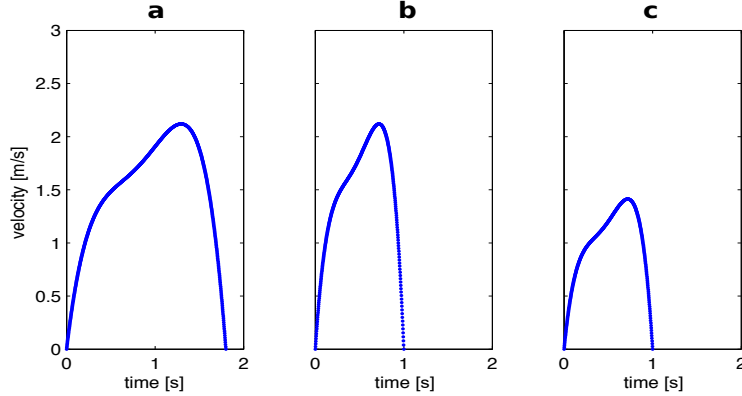
Figure 3: Acquisition of normalized velocity segments. The curve in panel (a) denotes the original velocity segment of a human participant, whereas that in panel (b) is obtained by normalizing the curve in panel (a) over the time interval $[0, 1]$. Finally, the normalized velocity segment in panel (c) is obtained after dividing the curve in panel (b) by the area between the curve and the time axis.

solutions to the system of nonlinear equations is investigated in theory, and numerical methods to determine the unknown coefficients for the desired base segment of velocity are discussed.

It has been demonstrated that smooth point-to-point movements can be generated by minimizing the time integral of the jerk magnitude squared [30]. This can be formulated as the following minimization problem:

$$\min_{x} J(x) \tag{2}$$

where

$$J(x) = \frac{1}{2} \int_{0}^{1} \left(\frac{d^3 x}{dt^3} \right)^2 dt$$

with $x(t), t \in [0, 1]$ denoting a desired position trajectory. An ideal solution to optimization problem (2) is given by a fifth-order polynomial in t (see Appendix 6.1 for the derivation).

$$x(t) = \sum_{i=0}^{5} a_i t^i, \quad t \in [0, 1] \tag{3}$$

where $a_i, i \in \{0, 1, 2, 3, 4, 5\}$ represent unknown coefficients. Therefore, the desired velocity segments correspond to a fourth-order polynomial in t.

Then the aim is to create a base segment of velocity that combines smooth point-to-point motion with the desired kinematic feature, which is described by the skewness and kurtosis of base segment of velocity. Thus, a fourth-order polynomial function in t is introduced, and it can

7

be regarded as a probability density function as follows

$$f(t) := \sum_{i=0}^{4} b_i t^i, \quad t \in [0, 1] \tag{4}$$

where $b_i, i \in \{0, 1, 2, 3, 4\}$ represent unknown coefficients, and with the following boundary conditions

$$f(0) = f(1) = 0 \tag{5}$$

Mean value μ and variance σ^2 of $f(t)$ are defined as follows:

$$\mu := \int_0^1 \tau f(\tau) d\tau, \quad \sigma^2 := \int_0^1 (\tau - \mu)^2 f(\tau) d\tau \tag{6}$$

Since the integral of $f(t)$ over the time interval $[0, 1]$ (i.e., the area of the base segment) must be unitary, that is

$$\int_0^1 f(\tau) d\tau = 1 \tag{7}$$

Equations (5), (6) and (7) yield $b_0 = 0$ and the following matrix equation

$$\begin{pmatrix} 1 & 1 & 1 & 1 \\ \frac{1}{2} & \frac{1}{3} & \frac{1}{4} & \frac{1}{5} \\ \frac{1}{3} & \frac{1}{4} & \frac{1}{5} & \frac{1}{6} \\ \frac{1}{4} & \frac{1}{5} & \frac{1}{6} & \frac{1}{7} \end{pmatrix} \mathbf{b} = \begin{pmatrix} 0 \\ 1 \\ \mu \\ \mu^2 + \sigma^2 \end{pmatrix} \tag{8}$$

where $\mathbf{b} = (b_1, b_2, b_3, b_4)^T$. Likewise, the definitions of skewness s and kurtosis k

$$s := \frac{1}{\sigma^3} \int_0^1 (\tau - \mu)^3 f(\tau) d\tau, \quad k := \frac{1}{\sigma^4} \int_0^1 (\tau - \mu)^4 f(\tau) d\tau \tag{9}$$

are respectively equivalent to

$$\mathbf{b}^T \begin{pmatrix} \frac{1}{5} - \frac{3\mu}{4} + \frac{2\mu^2}{3} \\ \frac{1}{6} - \frac{3\mu}{5} + \frac{\mu^2}{2} \\ \frac{1}{7} - \frac{\mu}{2} + \frac{2\mu^2}{5} \\ \frac{1}{8} - \frac{3\mu}{7} + \frac{\mu^2}{3} \end{pmatrix} = s\sigma^3 \tag{10}$$

and

$$\mathbf{b}^T \begin{pmatrix} \frac{1}{6} - \frac{4\mu}{5} + \frac{3\mu^2}{2} - \mu^3 \\ \frac{1}{7} - \frac{2\mu}{3} + \frac{6\mu^2}{5} - \frac{3\mu^3}{4} \\ \frac{1}{8} - \frac{4\mu}{7} + \mu^2 - \frac{3\mu^3}{5} \\ \frac{1}{9} - \frac{\mu}{2} + \frac{6\mu^2}{7} - \frac{\mu^3}{2} \end{pmatrix} = k\sigma^4 \tag{11}$$

8

By substituting $\mathbf{b}$ in Equations (10) and (11) with the solution to Equation (8), a fourth-order polynomial system with two variables (μ and σ) and two parameters (s and k) is obtained as follows

$$\begin{cases} \mathcal{F}(\mu, \sigma, s) = 0 \\ \mathcal{G}(\mu, \sigma, k) = 0 \end{cases} \tag{12}$$

where $\mathcal{F}(\mu, \sigma, s) = 0$ and $\mathcal{G}(\mu, \sigma, k) = 0$ correspond to (10) and (11), respectively. The following result holds for the solution to system (12).

Proposition 2.1. *There exist real solutions μ and σ to the polynomial system (12) for any given positive parameters s and k characterizing the motor signature of a human player.*

Proof. See Appendix 6.2. $\square$

Proposition 2.1 guarantees the existence of base segments of velocity satisfying smooth point-to-point movements with specified skewness and kurtosis. Nevertheless, the solutions are not unique. If multiple (μ, σ) pairs are the real zeros, the pair that is the closest to the mean value and the standard deviation of the normalized velocity segment of the given human player is selected as the desired solution. In addition, analytical solutions to the polynomial system (12) are not always available, hence numerical methods (*i.e.*, polynomial continuation) have to be used to find approximate solutions of mean value μ and standard deviation σ for given skewness s and kurtosis k. By means of approximated values of mean μ and standard deviation σ, it is feasible to obtain the coefficient vector $\mathbf{b} = (b_1, b_2, b_3, b_4)^T$ and the base segment of velocity $f(t)$ via Equation (8).

3 Control Architecture

The *in-silico* generation of velocity trajectories in solo motion with prescribed kinematic features allows to develop a customized VP able to interact with a HP in JI condition, with the former exhibiting the desired motor signature of a given human participant. This section presents the control architecture of the VP to shed light on the relationship between the mechanism underlying the generation of solo and joint improvised motions. Compared with previous approaches [19, 20, 23], the proposed one in this work allows the VP to spontaneously reproduce the motor signature of a given HP, without making use of pre-recorded time series of her/his motion in solo condition. This overcomes the drawback given by the need for a large database of human solo trajectories, and endows the VP with a wider repertoire of motor signatures, thus opening
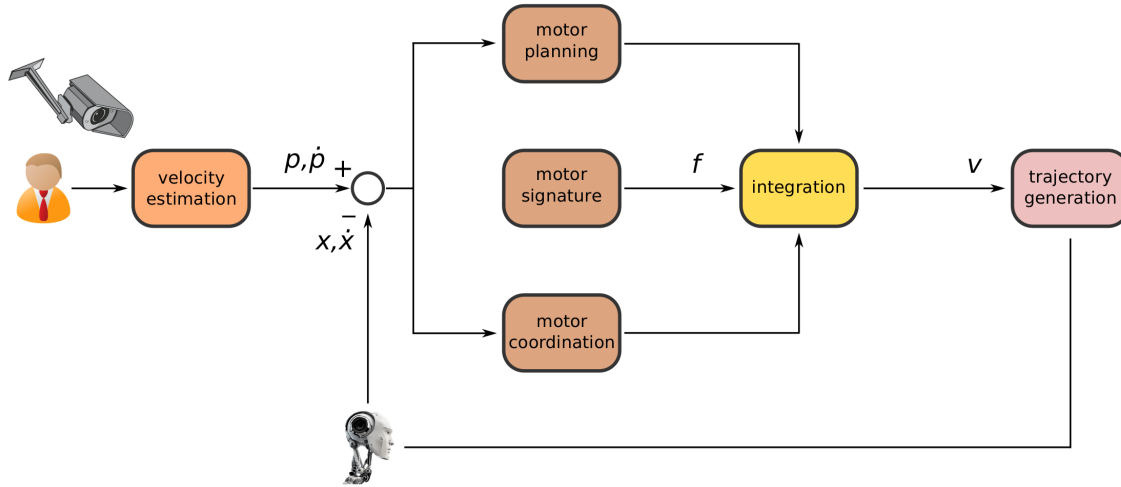
Figure 4: Control architecture of the VP in the mirror game. Variables p and $\dot{p}$ represent position and velocity of the HP, while x and $\dot{x}$ those of the VP; f represents the base segment and v the actual velocity segment of the VP, respectively.

the possibility of exploring the effects of continuously changing its kinematic features during the interaction with another partner.

The proposed control architecture (shown in Fig. 4) consists of six function blocks described in details as follows.

1. Velocity Estimation: The position trajectory of a HP detected by a camera is sent to this block, where her/his corresponding velocity time series is estimated and split into a series of velocity segments [18]. Then position and velocity errors between HP and VP are computed.

2. Motor Planning: This block determines the direction, duration and displacement of the velocity segments for the VP.

3. Motor Signature: This block reflects the kinematic features of a given HP as it generates the base segment of velocity f. It allows to change the motor signature of the VP by resetting the desired values of μ, σ, s and k.

4. Motor Coordination: This block allows for mutual adaptation, imitation and synchronization between the VP and its partner in joint improvisation condition.

5. Movement Integration: The actual velocity segments v of the VP are generated by integrating the movement constraints on motor planning, motor signature and motor coordination.

6. Trajectory Generation: The movement trajectory of the VP is generated by chronologically assembling the integrated velocity segments.

3.1 Generation of solo motions

While playing the mirror game in solo condition, the VP produces a prescribed motion without taking into consideration that of any other participant. Specifically, the actual segments of velocity v are derived from the the base segments f after integrating the displacement with the duration of time, and after assigning a motion direction.

Let Δt denote the duration of the time interval for each velocity segment, which is a random variable with probability density function $\lambda(\tau)$ that can be obtained by statistically analyzing the solo recordings of a human participant. The probability of Δt belonging to the interval $[\underline{t}, \bar{t}]$ can be calculated as

$$P\left(\underline{t} \leq \Delta t \leq \bar{t}\right) = \int_{\underline{t}}^{\bar{t}} \lambda(\tau) d\tau \tag{13}$$

According to experimental data, the average time interval for velocity segments is equal to 0.8s, with a standard deviation of 0.7s [18]. In addition, Δl represents the segment displacement (i.e., position mismatch between the starting point and terminal point of each segment), which is a random variable with probability density function $\xi(s)$. Likewise, the probability of Δl belonging to the interval $[\underline{l}, \bar{l}]$ is given by

$$P\left(\underline{l} \leq \Delta l \leq \bar{l}\right) = \int_{\underline{l}}^{\bar{l}} \xi(s) ds \tag{14}$$

Regardless of the motion direction, the variant of a base segment can be calculated as

$$\frac{\Delta l}{\Delta t} \cdot f\left(\frac{t}{\Delta t}\right) \tag{15}$$

where f is defined in Equation (4). Figure 5 shows a base segment of velocity and its possible eight variants with respect to time duration Δt and displacement Δl.

Since HPs tend to move around the middle part of the string in solo trials [17], the movement direction of the VP is determined by

$$\vec{D} = \begin{cases} \text{sign}(x - p_b), & |x - p_a| > |x - p_b|; \\ \text{sign}(x - p_a), & |x - p_a| < |x - p_b|; \\ \text{either}, & |x - p_a| = |x - p_b|, \end{cases} \tag{16}$$
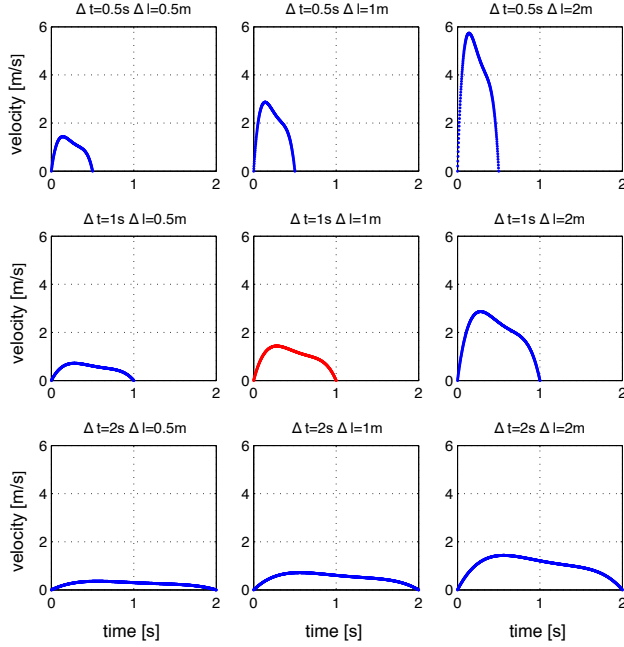
11

Figure 5: Variants of a base segment of velocity with respect to time duration Δt and displacement Δl. The red curve represents $f(t)$, while the blue ones represent its variants obtained for different values of Δt and Δl as described in Equation (15).

where x denotes the position of the VP, and $p_a < p_b$ represent position bounds. An actual velocity segment v is then constructed as follows

$$v(t) = \vec{D} \cdot \frac{\Delta l}{\Delta t} \cdot f\left(\frac{t}{\Delta t}\right) \quad t \in [0, \Delta t] \tag{17}$$

Solo motions are generated by consecutively joining the actual velocity segments together. Finally, the position trajectory of the VP is produced as follows

$$x(t) = x_0 + \int_0^t v(\tau)d\tau \quad t \in [0, \Delta t] \tag{18}$$

where x_0 denotes the initial position of the generated trajectory. Table 1 summarizes the solo motion algorithm (SMA) employed for the VP to produce human-like solo movements with prescribed kinematic features. In theory, there is a singularity in the acceleration profile when the two velocity segments with different slopes at the boundary are joined together. The mathematical methods such as polynomial interpolation can be used to remove this singularity by constructing an interpolation polynomial around the singularity. In this work, the method of polynomial interpolation is not adopted in numerical simulations because it dose not have much impact on solo motions when the length of interpolation interval is relatively small (normally

Table 1: Solo Motion Algorithm (SMA).

1: Set skewness s, kurtosis k and running time T_s
2: Generate a base segment $f(t)$ with (4)
3: **while** (time $< T_s$)
4:       Determine the segment duration Δt with (13)
5:       Determine the segment displacement Δl with (14)
6:       Choose the movement direction $\vec{D}$ with (16)
7:       Generate an actual velocity segment $v(t)$ with (17)
8:       Output the position trajectory $x(t)$ with (18)
9: **end while**

less than 0.01s). In addition, the singularity issue occurs due to the nonexistence of the instant acceleration at the boundary. The SMA is implemented by directly assembling velocity segments, which is not directly related to the instant acceleration. Thus, it does not cause the trouble in numerical simulations.

3.2 Generation of joint improvised motions

While playing the mirror game in JI condition, the VP interacts with its partner while exhibiting some prescribed kinematic features (motor signature). Based on the position and velocity mismatch between the two players, the proposed control architecture allows the VP to imitate, adapt to and synchronize with the movement of its partner, thereby achieving joint improvisation [20].

Similarly to the SMA, the segment duration and displacement are determined by Equations (13) and (14), respectively. As the two participants attempt to achieve movement synchronization, the movement direction of the VP is given by

$$\vec{D} = \text{sign}(p - x) \tag{19}$$

where x denotes the position of the VP and p refers to that of the other agent. When $p = x$, the VP is provided with a random direction.

The motor coordination block enables the VP to imitate and adapt to the movement of its partner in order to synchronize their joint movements, while the two participants consciously

adjust their way of moving (i.e., the profile of their velocity segments during the game). It has been suggested that an optimal feedback control driving the VP is equivalent to a PD control when the optimization interval is small enough, and that the nonlinear HKB equation originally introduced in [25] is not significantly better than a double integrator as end effector model of the VP in the mirror game [32].

For the sake of simplicity, a double integrator with PD control is employed to describe the motion of the VP and design the online algorithm as follows

$$\ddot{x} = c_s(v - \dot{x}) + c_v(\dot{p} - \dot{x}) + c_p(p - x) + \kappa(x, \epsilon) \tag{20}$$

where v is the actual velocity segment generated by Equation (17), x and $\dot{x}$ represent position and velocity of the VP, p and $\dot{p}$ those of its partner, with c_s, c_v and c_p being tunable positive parameters. The first three terms on the right-hand side of Equation (20) account for preferred movement, mutual imitation and movement synchronization, respectively [20], whereas $\kappa(x, \epsilon)$ is used to constrain the movement of the VP within the admissible range of motion:

$$\kappa(x, \epsilon) = \begin{cases} c_r|x - p_b|, & x - p_a \leq \epsilon \\ -c_r|x - p_a|, & p_b - x \leq \epsilon \\ 0, & \text{otherwise} \end{cases}$$

with c_r and ϵ being tunable positive parameters. When the distance between the VP and its closer bound is lower than ϵ, the term $\kappa(x, \epsilon)$ drives the VP with strength c_r towards the middle point of the position range. While implementing the online algorithm (20), the position of VP's partner is detected at each sampling period and the velocity can be estimated using the first-order backward difference method. Then mismatches of position and velocity are calculated to obtain the acceleration of the VP.

By solving equation (20), the position trajectory of the VP is given by

$$x(t) = x_0 + \int_0^t \int_0^\tau \ddot{x}(s)ds \, d\tau, \quad t \geq 0 \tag{21}$$

where x_0 refers to the initial position of the VP. Table 2 summarizes the joint improvisation algorithm (JIA) employed for the VP to perform JI with another agent in the mirror game.

In theory, the SMA generates a specific solo time series with a determinate probability. For the given initial conditions of position, velocity and acceleration, the JIA also produces a specific movement trajectory with a determinate probability. Thus, the proposed algorithms are statistically stable (see Appendix 6.3 for the detailed analysis).

14

Table 2: Joint Improvisation Algorithm (JIA).

1: Set skewness s, kurtosis k and running time T_s

2: Generate a base segment $f(t)$ with (4)

3: **while** (time $< T_s$)

4:       Determine the segment duration Δt with (13)

5:       Determine the segment displacement Δl with (14)

6:       Choose the movement direction $\vec{D}$ with (19)

7:       Generate an actual velocity segment $v(t)$ with (17)

8:       Compute the acceleration $\ddot{x}(t)$ with (20)

9:       Output the position trajectory $x(t)$ with (21)

10: **end while**

---

4 Experimental Validation

In order to validate the proposed approach, this section compares solo and joint improvised motions of human players with those generated by their respective customized virtual agents.

4.1 Metrics

In order to quantify the global performance of HP and VP in solo and joint improvisation conditions, the following indices are introduced: root mean square error (RMSE) of the position time series, circular variance (CV) and similarity level (SL) of normalized velocity segments. Their definitions are given as follows.

1. RMSE: The root mean square error of the position time series describes the temporal correspondence between two interacting players [26]:

$$RMSE = \sqrt{\frac{1}{n} \sum_{j=1}^{n} (x_{1,j} - x_{2,j})^2} \qquad (22)$$

where n is the number of sampling steps in the simulation, and $x_{1,j}$ and $x_{2,j}$ denote the positions of the two players at the jth sampling step, respectively. Lower values of RMSE indicate better temporal correspondence.

2. CV: The circular variance is used to quantify the coordination level between two interacting players [33]:

$$CV = \left\| \frac{1}{n} \sum_{j=1}^{n} e^{i\Delta\Phi_j} \right\| \quad \in [0,1] \tag{23}$$

where $\Delta\Phi_j$ represents the relative phase between the two players at the jth sampling step, n refers to the total number of time steps, and $\| \cdot \|$ denotes the 2-norm. Higher values of CV are representative of higher coordination levels between the two players.

3. SL: The similarity level describes the similarity degree between two time series of velocity in terms of averaged skewness and kurtosis of normalized velocity segments:

$$SL = \sqrt{(\bar{s}_1 - \bar{s}_2)^2 + (\bar{k}_1 - \bar{k}_2)^2} \tag{24}$$

where $\bar{s}_i = \frac{1}{n_i} \sum_{j=1}^{n_i} s_{i,j}$ and $\bar{k}_i = \frac{1}{n_i} \sum_{j=1}^{n_i} k_{i,j}$, $i \in \{1, 2\}$. Specifically, $\bar{s}_i$ and $\bar{k}_i$ denote the averaged skewness and kurtosis of normalized velocity segments from the ith velocity time series, respectively, whereas n_i represents the number of velocity segments in the ith time series of velocity. In addition, $s_{i,j}$ and $k_{i,j}$ refer to the skewness and kurtosis of the jth normalized velocity segment in the ith time series of velocity. Lower values of SL are representative of higher similarity degree between two time series of velocity.

To investigate the individual parts of the JI motions, the co-confident (CC) motions and jitter motions are taken into account in the analysis [9, 18]. The jitter motions describe the inability of the follower to precisely track the motion of the leader or the unfitness of the novices to enter the co-leadership state with the expert [9, 18]. And it is quantified by the relative Fourier root-mean-square(rms) power in the 2-3Hz band [9]. In addition, the co-confident motions mainly consider the highly synchronized periods [9, 18]. For simplicity, the alternative definition of CC motions is adopted to identify the highly synchronized periods in the JI motions [18].

4.2 Experimental set-up

Two different test conditions are developed to validate the human-like performance of a VP driven by the proposed control architecture: solo motions and joint improvised motions, in both HP-VP interaction and VP-VP interaction. The numerical algorithms in the control architecture are implemented in Matlab R2010a, and the Matlab function "fsolve" is employed to solve the systems of nonlinear equations (12) and determine the unknown coefficients of base segment of velocity. The solo motions are generated by the SMA with the motor signature of a given HP.
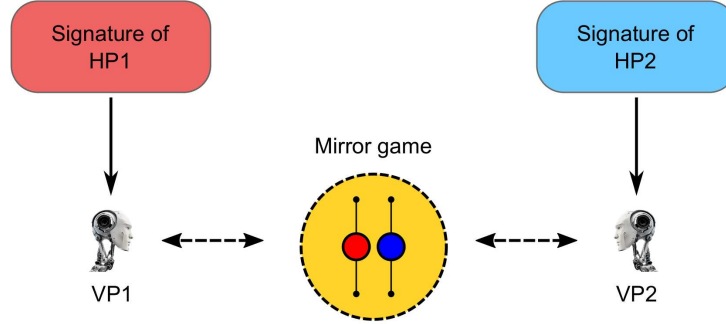
16

Figure 6: Schematic diagram for VP-VP interaction.

Statistical comparisons are carried out between the simulated solo motions and the solo motions of the given HP.

The joint improvised motions of a VP are produced by the JIA. For the experimental test of HP-VP interaction, the HP is required to sit in front of a laptop, which implements the JIA in Matlab. The blue ball on the laptop screen represents the position of the HP, which is controlled by means of a mouse, while the red one represents that of the VP, which is generated by the JIA. In fact, the mouse setup is only used to preliminarily look at whether the algorithm is able to interact with the HP in the mirror game. Eventually, the computer avatar of the HP (typically the patient with mental impairments) will be created using the technology of virtual reality. And the algorithm will be integrated with the computer avatar to play the mirror game with the patient with the help of doctors in the hospital.

The schematic diagram of VP-VP interaction in joint improvisation condition is presented in Fig. 6. Finally, the focus is on validating the two customized VPs' capability of reproducing the kinematic characteristics observed when two HPs play together in the mirror game. The validation method is the same as that proposed in [20]. Specifically, two virtual players (VP1 and VP2) are enabled to play the mirror game in a JI condition, with VP1 (VP2) being fed with the motor signatures of HP1 (HP2), respectively.

4.3   Solo motions

Figures 7(a) and 7(b) show position and velocity time series of a HP performing a 60s solo trial. The HP moves the ball along the string within the normalized range $[-1, 1]$. The sampling frequency of the camera is 100 Hz. According to data analysis of the velocity segments shown in Fig. 7(b), the averaged mean value $\bar{\mu}$, standard deviation $\bar{\sigma}$, skewness $\bar{s}$ and kurtosis $\bar{k}$ are
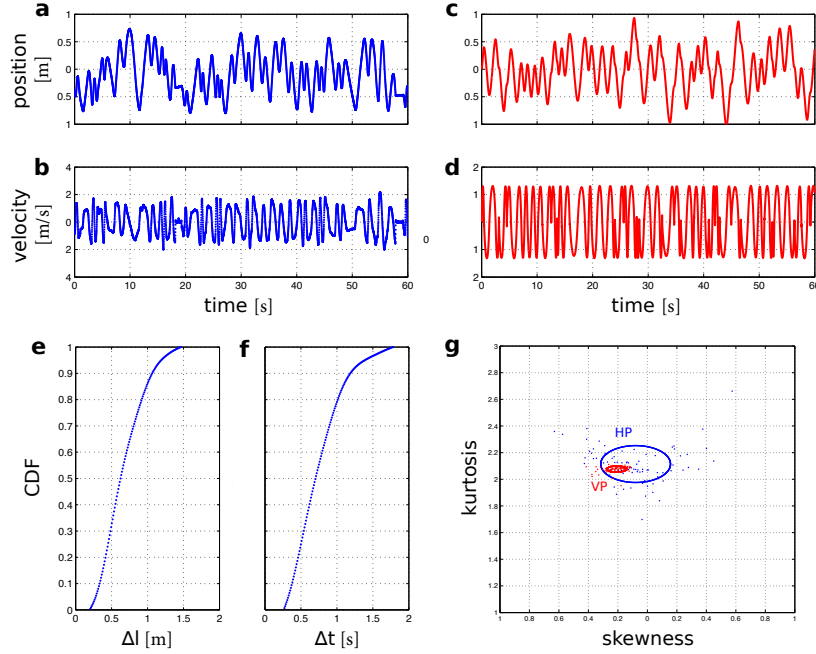
Figure 7: Experimental test – solo motions. Position (a) and velocity (b) time series of the HP. Position (c) and velocity (d) time series of the VP. CDFs of Δl (e) and Δt (f) for the HP. (g) Visualization of solo motion for the HP and her/his customized VP in the S-K plane: blue dots correspond to velocity segments of the HP, whereas red ones refer to those of the VP. The two corresponding ellipses are evaluated by means of Equation (1).

0.50, 0.23, -0.08 and 2.11, respectively.

The probability distributions of Δl and Δt of the velocity segments in Fig. 7(b) are described by cumulative distribution functions (CDF) shown in Figs. 7(e) and 7(f), respectively.

Figures 7(c) and 7(d) show position and velocity time series of a VP fed with the same motor signature as that in Fig. 7(b) and driven by the SMA described in Table 1. The velocity segments generated by the SMA resemble those of the HP in terms of profile, yet are slightly smoother. A visible difference is that the HP sometimes stays still during the game, whilst the VP always keeps moving.

Figure 7(g) shows skewness and kurtosis of normalized velocity segments for both the HP and her/his customized VP in the S-K plane. It is possible to appreciate that most velocity segments of the VP are mapped into the ellipse representing the kinematic features of the HP, thus confirming that the VP succeeds in reproducing the motor signature of the specified HP. Moreover, the VP segments are clustered together, whereas those of the HP are scattered in the
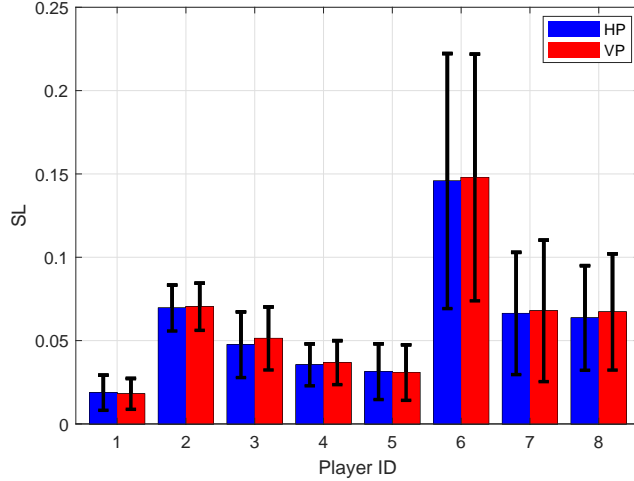
Figure 8: Statistical validation of the SMA. The height of the bars denotes the mean value of SL, whereas the black error bar refers to its standard deviation.

S-K plane, thus implying that solo motions of human players are more flexible and diverse than those of their customized computer avatar. In fact, one solo trial generated by the SMA is not sufficient to evaluate the performance of the VP. Thus, the statistical analysis is conducted to make a comparison between simulation results and the benchmark.

4.3.1 Statistical analysis

In order to validate the solo motions generated by the SMA, 8 HPs are asked to play the mirror game in solo condition. Each HP is required to play 3 times in the experiment. For each HP, the skewness and kurtosis of normalized velocity segments in solo trials are computed. Afterwards the benchmark using experimental data in human solo trials is introduced. Specifically, the SL values of any two solo trials are computed for each HP to obtain the mean value and standard deviation of SL, which are regarded as the benchmark of each HP (see the blue bars and their respective error bars in Fig. 8). For the solo trials of each HP, the SMA generates the corresponding solo motions by regarding their respective averaged skewness and kurtosis as the motor signature. Similarly, the SL values of any two solo motions generated by the SMA are computed for each customized VP to obtain the mean value and standard deviation of SL (see the red bars and their respective error bars in Fig. 8). In terms of the mean values of SL, the customized VPs fluctuate by -3.7%, 1.1%, 7.9%, 3.7%, -1.7%, 1.5%, 2.4%, 5.7% with respect to their respective benchmarks (blue bars) from Player 1 to Player 8. For the standard

19

deviations of SL, the corresponding fluctuation ratios are -12.2%, 2.7%, -4.1%, 4.9%, -0.4%, -3.3%, 15.8%, 11.2%, respectively. This indicates the capability of the SMA to generate the solo motions with the personalized motor signature.

4.4 Joint improvised motions

This section presents the experimental test of the JIA described in Table 2 for both HP-VP and VP-VP interactions. The experimental test allows to look at whether the VP is able to generate the joint improvised motion and socially interact with its partner (HP or VP). In addition, the validation of the JIA is also conducted by tuning the parameters of VPs to match the experimental data.

4.4.1 HP-VP interaction

The parameter setting for the VP is given as follows: $\bar{\mu} = 0.51$, $\bar{\sigma} = 0.23$, $\bar{s} = -0.09$, $\bar{k} = 2.14$, $c_s = 2$, $c_v = 5$, $c_p = 3$, $c_r = 5$ and $\epsilon = 0.1$. Specifically, the parameters $\bar{\mu}$, $\bar{\sigma}$, $\bar{k}$ and $\bar{s}$ are selected based on the solo trial of the HP. The parameters c_s, c_v and c_p are tuned to increase the CV value and decrease the values of $RMSE$ and SL. In addition, c_r and ϵ are tentatively selected to avoid the collision with the boundaries. Figures 9(a) and 9(b) show position and velocity time series of HP and VP with $RMSE = 0.096$ and $CV = 0.972$, respectively. Some synchronized segments can be observed in the position trajectories, which implies the occurrence of joint improvisation between HP and VP. The two ellipses featuring the movement patterns of the two interacting agents are shown in Fig. 9(c). It is possible to appreciate that they are largely overlapping in the S-K plane with $SL = 0.219$, implying that the two players exhibit similar kinematic features while interacting in the mirror game.

4.4.2 VP-VP interaction

The two VPs are driven by the JIA with the following parameters setting: $\bar{\mu}_1 = 0.51$, $\bar{\sigma}_1 = 0.22$, $\bar{s}_1 = -0.18$ and $\bar{k}_1 = 2.13$ for VP1, $\bar{\mu}_2 = 0.53$, $\bar{\sigma}_2 = 0.25$, $\bar{s}_2 = -0.18$ and $\bar{k}_2 = 1.87$ for VP2, and $c_s = 1.5$, $c_v = 3.6$, $c_p = 4.9$, $c_r = 5$ and $\epsilon = 0.1$ for both VPs. The parameters $\bar{\mu}_i$, $\bar{\sigma}_i$, $\bar{k}_i$ and $\bar{s}_i$, $i \in \{1, 2\}$ are selected according to the solo trials of two HP, respectively. The parameters c_s, c_v and c_p are tuned so that the performance of the customized VP pair matches that of the HP pair as much as possible (The values of $RMSE$, CV and SL from the customized VP pair are close to those from the HP pair). The values of c_r and ϵ are the same as those in the HP-VP
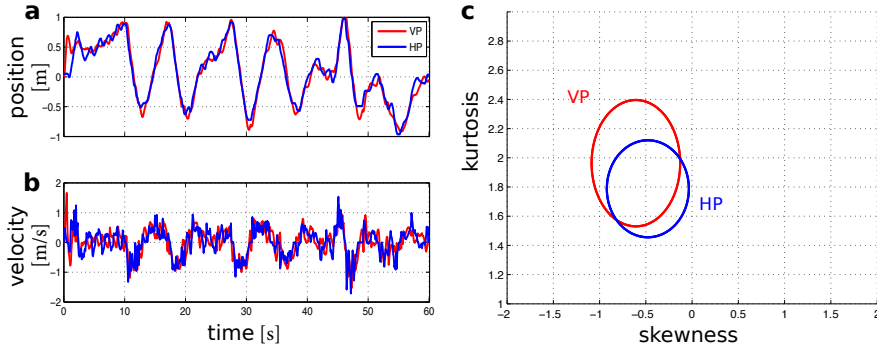
Figure 9: Experimental test – JI trial between HP (blue) and VP (red). Position (a) and velocity (b) time series of HP and VP. (c) Visualization of the JI motion between HP and VP in the S-K plane.

interaction. Figures 10(a) and 10(b) show position and velocity time series of the two HPs with $RMSE = 0.135$ and $CV = 0.775$, while Figures 10(c) and 10(d) those of the two customized VPs with $RMSE = 0.042$ and $CV = 0.989$, respectively. VP1 and VP2 succeed in reproducing the joint improvised movement (synchronized segments) as occurred in the HP1-HP2 interaction.

Figure 10(e) describes the transition of motor signatures from solo to JI motion. The kinematic features of the HPs in solo condition are separate, while those in JI condition converge towards each other with $SL = 0.079$ and are more variable. Notably, similar remarks can be made for the kinematic features exhibited by the VPs with $SL = 0.094$, thus indicating the desirable matching performance of the VPs driven by the proposed control architecture.

4.4.3 Statistical analysis

To further validate the JIA, 4 Dyads are investigated, with each dyad including a HP-HP pair and a VP-VP pair. Specifically, three JI trials are conducted for each HP-HP pair in the experiment. Then the mean values and standard deviations of RMSE, CV and SL are computed for the JI trials. The above values are regarded as the benchmark for the validation of VP-VP interaction. Next, the parameters c_s, c_v and c_p are tuned for each VP-VP pair to match the benchmark of the HP-HP pair (see Appendix 6.4 for more details). In addition, $c_r = 5$ and $\epsilon = 0.1$ remain unchanged in the validation of all VP-VP pairs. Essentially, each VP is equipped with the motor signature of a given HP to act as her/his avatar in the simulation.

Figure 11 presents matching results of VP-VP pairs with respect to their benchmarks (*i.e.*, HP-HP pairs) in JI condition. It is possible to appreciate that the VP-VP pairs statistically
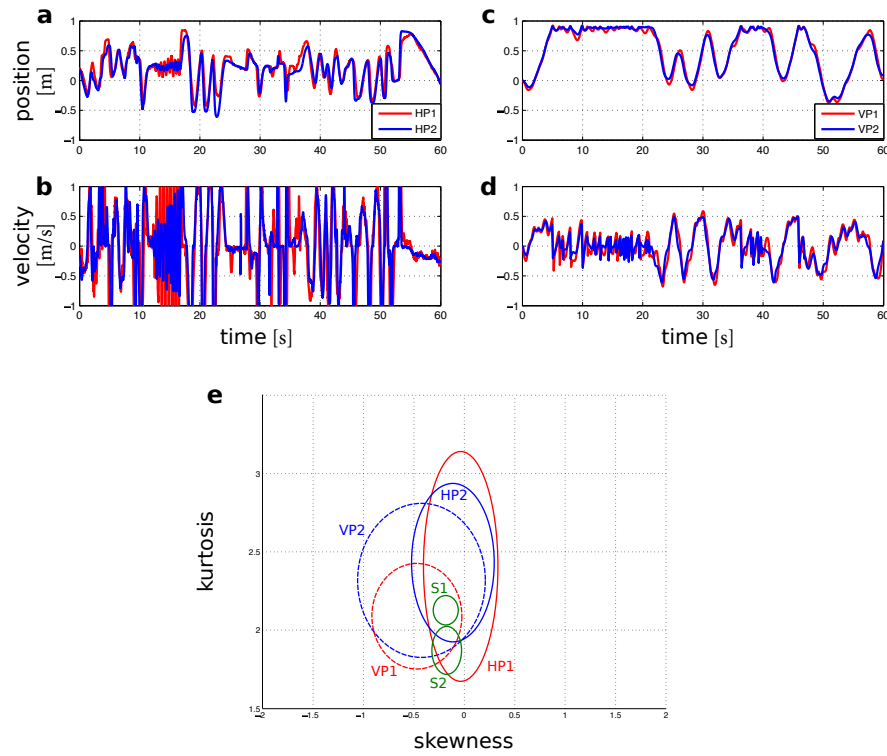
21

Figure 10: Experimental test – JI trial in a human (HP1 and HP2) and in a virtual (VP1 and VP2) dyad. Position (a) and velocity (b) time series of the human dyad (HP1 in red and HP2 in blue). Position (c) and velocity (d) time series of the virtual dyad (VP1 in red and VP2 in blue). (e) Visualization of solo and JI motions for the human pair and the customized virtual pair in the skewness-kurtosis plane. VP segments are mapped into dashed-line ellipses (VP1 in red and VP2 in blue), HP segments into solid-line ellipses (HP1 in red and HP2 in blue), and their corresponding kinematic signatures in solo motion (S1 and S2) into green solid-line ellipses.
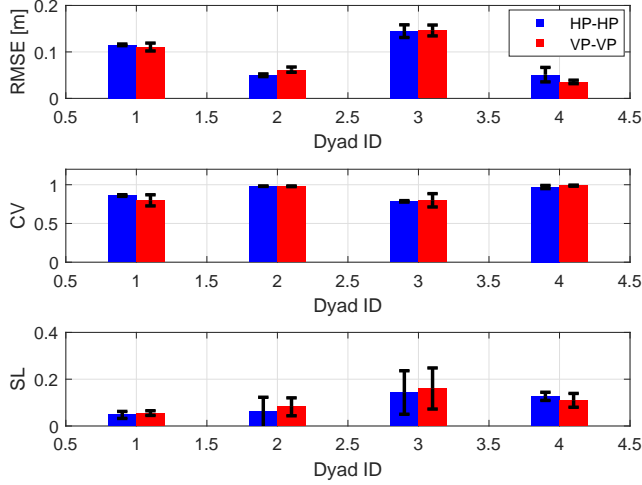
Figure 11: Statistical validation of the JIA. Mean values are represented by the height of each rectangle, whereas standard deviations are represented by black error bars. The blue rectangles and their error bars characterize the kinematic feature of HP-HP pairs in terms of RMSE (top), CV (middle) and SL (bottom), which is viewed as the benchmark. The red rectangles and their error bars quantify the respective statistical performance of VP-VP pairs through tuning the parameters of the proposed mathematical model.

behave like the HP-HP ones. To be specific, for the RMSE, the VP-VP pair (red rectangle) is slightly higher than its benchmark (blue rectangle) with a marginal increment of 0.022 in Dyad 2 but lower than the benchmark with a tiny decrement of 0.017 in Dyad 4. In addition, the error bars of VP-VP pairs are also close to those of their respective HP-HP pairs with the maximum mismatch of 0.012 in Dyad 4. As for the CV, the VP-VP pairs achieve excellent matching results with the height mismatch between blue rectangles and red ones less than 0.062 for all dyads, except for slightly large error bars with the increments of 0.061 in Dyad 1 and 0.077 in Dyad 3, respectively. Finally, for the SL, the VP-VP pairs succeed in reproducing the features of HP-HP pairs in terms of both mean values (rectangle heights) and standard deviations (error bars). Specifically, the largest mismatch of mean values is 0.022, while that of standard deviations is 0.024, both in Dyad 2.

The CC motions and jitter motions are also considered to analyze and compare the individual parts in the JI motions. Let the index γ_{CC} denote the ratio of CC segments in the all segments for each JI trial. Clearly, the larger values of γ_{CC} indicate the more high-level synchronization

23

of individual parts in the JI motions. Figure 12 shows the statistics on the index γ_{CC} for each HP-HP pair and the customized VP-VP pair in the JI trials. On the whole, the values of γ_{CC} in Dyads 2 and 4 are much larger than those in Dyads 1 and 3, which indicates that the players in Dyads 2 and 4 perform better in terms of generating CC segments in the JI trials. The above observation is consistent with their global performance of JI motions in Figure 11, where Dyads 2 and 4 have the relatively larger values of CV and the relatively smaller values of RMSE, as opposed to Dyads 1 and 3. Notably, Dyad 2 is superior to Dyad 4 in generating the CC motions, though they have the similar global performance (i.e., RMSE, CV, SL) in the JI motions. In terms of matching performance, the height differences between the blue rectangle and the red one (i.e., mean values of γ_{CC}) in each dyad are 0.016, 0.171, 0.012 and 0.015 (from Dyad 1 to Dyad 4), respectively. Similarly, the length differences of black error bars (i.e., standard deviations of γ_{CC}) in each dyad are 0.006, 0.118, 0.009 and 0.029, respectively. Moreover, the jitter motions are observed in both HP-HP pairs (Dyads 1, 3 and 4) and VP-VP pairs (Dyads 1, 3 and 4). Nevertheless, there are no visible jitter motions in the JI trials of Dyad 2 (both HP-HP pair and VP-VP pair) due to the high-level coordination of players in this dyad. To characterize the extent of jitter motions, the proportions of jitter periods to the whole trial duration (i.e., 60s) are computed for each trial, which allows to obtain the mean values and standard deviations of the proportions for all HP-HP and VP-VP trials, respectively. The mean value and standard deviation of the proportion are respectively 0.036 and 0.048 for all the HP-HP trials, in contrast with the mean value 0.011 and the standard deviation 0.015 for all the VP-VP trials.

In [18], it is observed that the CC segments account for 16.5% of all segments. The analysis in this work leads to the different percentages: 13.9% for HP-HP trials and 9.9% for VP-VP trials. The percentage (13.9%) of CC segments for HP-HP trials in this work is slightly smaller than the value (16.5%) in [18]. The percentage difference probably results from the improvisation experience of players (i.e., expert players are better at generating CC segments compared to novices), and there are no expert players in this work. The relatively small percentage (9.9%) for VP-VP trials suggests that the proposed algorithm (i.e., JIA) does not generate enough highly synchronized segments. In addition, it is demonstrated that there exists the "universal CC region" around skewness 0 ± 0.04 and kurtosis 2.2 ± 0.02 [18]. The analysis of CC segments in this work allows to obtain the "universal CC region" around skewness -0.04 ± 0.06 (-0.08 ± 0.19) and kurtosis 2.1 ± 0.07 (2.2 ± 0.14) for HP-HP trials (VP-VP trials). In terms of region area, the "universal CC region" in [18] is the smallest. In contrast, the region generated by VP-VP trials in this work is the largest, and it covers the 'universal CC region" in [18] and overlaps with a
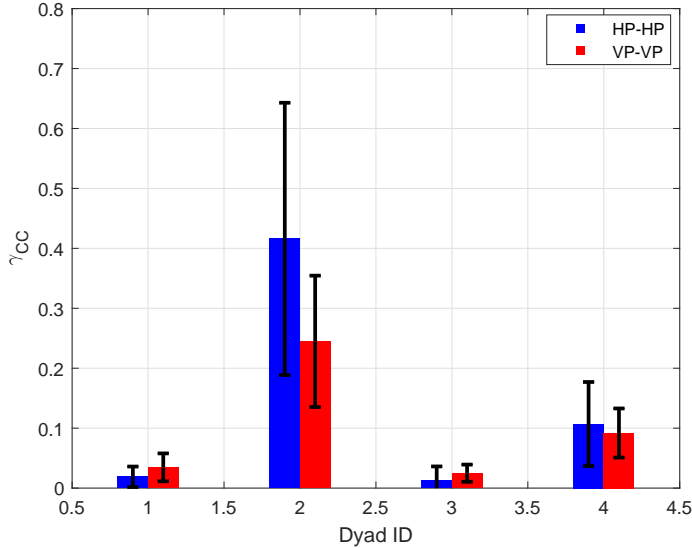
Figure 12: The ratios of CC segments in the all segments for the HP-HP and VP-VP trials. The rectangle height denotes the mean value of γ_{CC}, and the black error bar refers to its standard deviation.

large part of the region generated by HP-HP trials in this work. The above observations indicate the CC segments in [18] possess very similar velocity profiles, while the proposed algorithm (i.e., JIA) generates the CC segments with diverse velocity profiles in VP-VP trials. Compared with the "universal CC region" in [18], the region generated by HP-HP trials in this work contains the points with the relatively smaller values of skewness and kurtosis. This suggests that the players in HP-HP trials accelerate in a gradual manner in order to generate the CC motions, which might contribute to the accurate timing between two players. Moreover, the ratio of average duration of jitter periods in each trial duration (i.e., 60s) is around 0.04 in the JI trials [9], which is close to the ratio (0.036) for HP-HP trials in this work. In comparison, the ratio (0.011) for VP-VP trials is relatively small, which implies the proposed algorithm (i.e., JIA) generates fewer jitter motions in the JI trials.

5   Conclusions

In this paper, an interactive control architecture based on velocity segments is developed to account for the generation of human solo motions and joint improvised motions in the mirror game. The interactive control architecture is composed of six basic building blocks: velocity

25

estimation, motor planning, motor signature, motor coordination, movement integration and trajectory generation. The motor signature is characterized by the base segment of velocity, which is constructed by endowing the smooth point-to-point movement with the specified skewness and kurtosis. The motions of VP are generated by consecutively assembling and adjusting the base segments of velocity. The previous work regards the motor signature as a global feature of human solo movements, and the joint improvised motions are generated by directly capitalizing on the prerecorded time series in solo trials [19, 23, 26]. Control theory and techniques play a crucial role in modeling human movements in the mirror game. Specifically, the jitter motions are reproduced by a reactive-predictive controller [9]. The adaptive control endows the algorithm with high adaptability while generating joint motions [23], and the optimal control allows to reconcile the motor signature with the movement coordination [19]. In particular, the continuous role transition (e.g., from the leadership to the followership) can be easily achieved by tuning a parameter in the model [19]. In addition, the stability of numerical algorithms is guaranteed in theory [19, 23, 26]. Compared to previous methods, human movements are modeled in the mirror game with a new perspective on motor signature, which is regarded as a local feature (i.e., velocity segments) of solo movements. The solo motions are generated by consecutively combining velocity segments with the specific motor signature (i.e., skewness and kurtosis of the normalized velocity segments), which allows to obtain the unlimited solo motions with the given signature. The joint improvised motions can be generated by solving a simple differential equation with the classic PD control. Based on the proposed control architecture, two numerical algorithms are developed to generate the solo motion and joint improvisation motion of a given HP, respectively. The generated solo motion is reconciled with the movement of VP's partner via the feedback control to produce the joint improvisation motion. Thus, it provides a new insight into the shift of kinematic patterns from individuality to joint improvisation. Theoretical analysis is also presented to guarantee the existence of base segments of velocity characterizing any individual motor signature. Moreover, the proposed approach is validated by matching experimental data.

Future work may include the learning of social signature in joint actions, the emergence of creative and improvised motions through the mutual imitation and the generalization of this control architecture to other experimental paradigms for investigating social motor coordination, both in dyads [34] and in larger ensembles [35, 36, 37, 38].

6 Appendix

6.1 Solution to optimization problem (2)

In order to solve the optimization problem (2), one first computes

$$J(x + c\delta x) = \frac{1}{2} \int_0^1 \left(\frac{d^3 x}{dt^3} + c \frac{d^3 \delta x}{dt^3} \right)^2 dt$$

where c is a constant and $\delta x(t), t \in [0, 1]$ is a smooth curve with the constraints

$$\delta x(0) = \frac{d^2 \delta x(0)}{dt^2} = \frac{d^3 \delta x(0)}{dt^3} = 0 \tag{25}$$

and

$$\delta x(1) = \frac{d^2 \delta x(1)}{dt^2} = \frac{d^3 \delta x(1)}{dt^3} = 0 \tag{26}$$

Then one obtains the increment of $J(x)$

$$J(x + c\delta x) - J(x) = \frac{c}{2} \int_0^1 \frac{d^3 \delta x}{dt^3} \left(2 \frac{d^3 x}{dt^3} + c \frac{d^3 \delta x}{dt^3} \right) dt$$

that leads to

$$\lim_{c \to 0} \frac{J(x + c\delta x) - J(x)}{c} = \int_0^1 \frac{d^3 \delta x}{dt^3} \cdot \frac{d^3 x}{dt^3} dt$$

From Equations (25) and (26) it follows that

$$\int_0^1 \frac{d^3 \delta x}{dt^3} \cdot \frac{d^3 x}{dt^3} dt = - \int_0^1 \delta x \cdot \frac{d^6 x}{dt^6} dt$$

The optimal trajectory should then satisfy

$$\lim_{c \to 0} \frac{J(x + c\delta x) - J(x)}{c} = - \int_0^1 \delta x \cdot \frac{d^6 x}{dt^6} dt = 0 \tag{27}$$

Since δx can be an arbitrary function with initial condition (25) and terminal condition (26), Equation (27) leads to a sixth-order differential equation

$$\frac{d^6 x}{dt^6} = 0 \tag{28}$$

Thus, a solution to Equation (28) is given by

$$x(t) = \sum_{i=0}^5 a_i t^i, \quad t \in [0, 1]$$

with unknown coefficients $a_i, i \in \{0, 1, 2, 3, 4, 5\}$.

6.2 Proof of Proposition 2.1

In what follows, the details on the proof of Proposition 2.1 are presented.

Proof. $\mathcal{F}(\mu, \sigma, s)$ and $\mathcal{G}(\mu, \sigma, k)$ in Equation (12) can be simplified as follows:

$$\mathcal{F}(\mu, \sigma, s) = -\mu^3 - 3\mu\sigma^2 - s\sigma^3 + \frac{3}{2}\mu^2 + \frac{3}{2}\sigma^2 - \frac{9}{14}\mu + \frac{1}{14} \tag{29}$$

and

$$\mathcal{G}(\mu, \sigma, k) = 3\mu^4 + 6\mu^2\sigma^2 - k\sigma^4 - 6\mu^3 - 6\mu\sigma^2 + \frac{89}{21}\mu^2$$
$$+ \frac{5}{3}\sigma^2 - \frac{26}{21}\mu + \frac{5}{42} \tag{30}$$

which can be rewritten as

$$\mathcal{F}_1(\mu, \sigma, s) := \frac{\mathcal{F}(\mu, \sigma, s)}{\sigma^3}$$
$$= -s + \left(\frac{3}{28\sigma^2} - 3\right)\frac{\mu - 1/2}{\sigma} - \left(\frac{\mu - 1/2}{\sigma}\right)^3 \tag{31}$$

and

$$\mathcal{G}_1(\mu, \sigma, s) := \frac{\mathcal{G}(\mu, \sigma, k)}{\sigma^4}$$
$$= -k + \frac{1}{6\sigma^2} - \frac{1}{336\sigma^4}$$
$$+ \left(6 - \frac{11}{42\sigma^2}\right)\left(\frac{\mu - 1/2}{\sigma}\right)^2 + 3\left(\frac{\mu - 1/2}{\sigma}\right)^4. \tag{32}$$

From these representations, it is evident that if the system has a solution $(\mu, \sigma) \in \mathbb{C}^2$ then it also has a solution $(1 - \mu, -\sigma)$. Furthermore, with the aid of substitution

$$M = \frac{\mu - 1/2}{\sigma}, \quad \eta = \frac{1}{\sigma^2} \tag{33}$$

the expressions for $\mathcal{F}_1(\mu, \sigma, s)$ and $\mathcal{G}_1(\mu, \sigma, k)$ can be further simplified as

$$\mathcal{F}_1(M, \eta, s) = -s + \left(\frac{3}{28}\eta - 3\right)M - M^3 , \tag{34}$$

and

$$\mathcal{G}_1(M, \eta, k) = -k + \frac{1}{6}\eta - \frac{1}{336}\eta^2 + \left(6 - \frac{11}{42}\eta\right)M^2 + 3M^4, \tag{35}$$

respectively. By solving equation $\mathcal{F}_1(M, \eta, s) = 0$ with respect to η, one obtains

$$\eta = \frac{28}{3}\left(M^2 + 3 + \frac{s}{M}\right) \tag{36}$$

28

Substitution of Equation (36) into $\mathcal{G}_1(M, \eta, k) = 0$ yields

$$\mathcal{G}_2(M, s, k) = 0 \tag{37}$$

with

$$\mathcal{G}_2(M, s, k) = 8\,M^6 - 36\,M^4 - 80\,sM^3 + (63 - 27\,k)M^2 - 7\,s^2\,. \tag{38}$$

According to data analysis of human movements in the mirror game, skewness s and kurtosis k belong to the intervals $(-0.5, 0.5)$ and $(1.5, 3)$, respectively [18]. For any selection of values $s \in (0, 0.5)$ and $k \in (1.5, 3)$, Equation (37) has a positive zero $M = M_0$ in the interval $(0, 2\sqrt{3})$ due to the conditions

$$\mathcal{G}_2(0, s, k) < 0, \tag{39}$$

and

$$\mathcal{G}_2(2\sqrt{3}, s, k) = (8417 - 1920\sqrt{3}s) + 324(3 - k) + 7(1 - s^2) > 0\,.$$

Therefore, from Equation (36) it is clear that also η is positive, hence the second equation from (33) can be resolved in real numbers with respect to σ. The corresponding value for μ can be then found in the first equation from (33), which implies that $\mathcal{F}(\mu, \sigma, s) = 0$ and $\mathcal{G}(\mu, \sigma, k) = 0$ have real zeros μ and σ.

As mentioned above, aside of a zero $(\mu, \sigma) \in \mathbb{R}^2$, the pair $(1 - \mu, -\sigma) \in \mathbb{R}^2$ is also a zero for this system. Therefore the number of real zeros (counted in accordance with their multiplicities) is always even. The correspondence between the set of real zeros of this system and those of the polynomial (38) treated with respect to the variable M is straightforward: any real zero of the latter generates a pair of real zeros of the former.

To discover the exact number of real zeros of the univariate polynomial in M for any specialization of parameters (s, k), one has to establish the locus of its *discriminant curve* [31] in the (s, k)-plane. The discriminant of $\mathcal{G}_2$ with respect to M is a polynomial

$$\mathfrak{D}(s, k) = (6\,k - 5)^2(3\,k - 7)^4 - 8(1026\,k^2 - 4281\,k + 4655)(3\,k - 7)^2 s^2$$

$$+8(16902\,k^3 - 77679\,k^2 + 105588\,k - 36603)s^4 + 224(-5589\,k + 11789)s^6 + 1362704\,s^8$$

which is even in s. The discriminant curve $\mathfrak{D}(s, k) = 0$ separates in the (s, k)-plane the domains corresponding to polynomials $\mathcal{G}_2$ with distinct numbers of real zeros. Some sample parameter settings are presented in Table 3.

$\square$

Table 3: Numerical examples on the number of real zeros.

(s, k)	Number of real zeros of (38)	Number of real zeros of (29)-(30)	Sample zero (μ, σ) $\approx$
$(0.10, 1.60)$	6	12	$(0.751, 0.119)$
$(0.25, 1.60)$	4	8	$(0.758, 0.114)$
$(0.40, 1.60)$	2	4	$(0.762, 0.109)$
$(0.25, 2.00)$	4	8	$(0.760, 0.112)$
$(0.25, 2.40)$	2	4	$(0.762, 0.111)$

6.3   Stability of the algorithms

According to Equation (20), the interaction of VP-VP pair can be described by the following system of differential equations:

$$\begin{cases} \ddot{x}_1 + c_{v,1}(\dot{x}_1 - \dot{x}_2) + c_{s,1}\dot{x}_1 + c_{p,1}(x_1 - x_2) - \kappa(x_1, \epsilon) = c_{s,1}v_1 \\ \ddot{x}_2 + c_{v,2}(\dot{x}_2 - \dot{x}_1) + c_{s,2}\dot{x}_2 + c_{p,2}(x_2 - x_1) - \kappa(x_2, \epsilon) = c_{s,2}v_2 \end{cases} \tag{40}$$

where $\ddot{x}_i$, $\dot{x}_i$ and x_i are the acceleration, velocity and position of the i-th VP with the corresponding parameters $c_{s,i}$, $c_{v,i}$ and $c_{p,i}$, $i \in \{1, 2\}$. In addition, v_1 and v_2 are motor signatures for the two VPs generated by the SMA. For the given initial conditions of $\dot{x}_i$ and x_i, $i \in \{1, 2\}$, the solutions to Equation (40) depend on the time series v_1 and v_2. For the specific time series of v_1 and v_2, the equation (40) generates the determinate movement trajectories of VP-VP pair. Suppose the time series v_i is composed of n_i velocity segments, and each velocity segment is created based on Δl and Δt. Let p_i^k and q_i^k denote the probabilities of selecting the specific Δl according to (14) and selecting the specific Δt according to (13) for the k-th velocity segment of time series v_i, respectively. Since the generation of each velocity segment is independent, the probability of generating a specific time series v_i by the SMA is $\prod_{k=1}^{n_i} p_i^k q_i^k$, and the probability of generating a specific pair of time series v_1 and v_2 is $\prod_{k=1}^{n_1} p_1^k q_1^k \cdot \prod_{k=1}^{n_2} p_2^k q_2^k$. Since the solutions to Equation (40) depend on v_1 and v_2, the probability of generating the specific movement trajectories of VP-VP pair by the JIA is also $\prod_{k=1}^{n_1} p_1^k q_1^k \cdot \prod_{k=1}^{n_2} p_2^k q_2^k$. This implies that the equation (40) produces the specific movement trajectories of VP-VP pair with a determinate probability. Similarly, for the HP-VP interactions, the VP generates the specific movement trajectory with a determinate probability for the given time series of the HP. Thus, the proposed algorithms SMA and JIA are statistically stable.

Table 4: Parameter setting for VP-VP pairs.

Parameters		c_s	c_v	c_p
Dyad 1	VP1	2.0	3.2	4.8
	VP2	2.5	2.0	5.5
Dyad 2	VP1	1.2	3.0	5.8
	VP2	1.8	2.2	6.0
Dyad 3	VP1	4.2	2.0	3.8
	VP2	3.8	1.2	5.0
Dyad 4	VP1	1.0	1.6	7.4
	VP2	1.2	1.8	7.0

6.4 Parameter setting of c_s, c_v and c_p

The parameters of c_s, c_v and c_p for each VP are tuned by means of a trial-and-error approach to match the benchmark of HP-HP pair. Note that c_s, c_v and c_p are all positive and satisfy the constraints $c_s + c_v + c_p = 10$. The desirable matching results in Fig. 11 are obtained according to the parameter setting of c_s, c_v and c_p in Table 4. In Dyad 1, Dyad 2 and Dyad 4, the values of c_p are larger than those of c_s and c_v for both VP1 and VP2, which means that these two VPs pay more attention to temporal correspondence of position in such JI trials. In Dyad 3, the two VPs focus on the temporal correspondence of position and their own motor signatures in the JI trials since the values of c_s and c_p are much larger than those of c_v for both VPs.

Acknowledgment

References

[1] Boraston, Z., Blakemore, S.J., Chilvers, R. and Skuse, D., 2007. Impaired sadness recognition is linked to social interaction deficit in autism. *Neuropsychologia*, 45(7), pp.1501-1510.

[2] Couture, S.M., Penn, D.L. and Roberts, D.L., 2006. The functional significance of social cognition in schizophrenia: a review. *Schizophrenia bulletin*, 32(suppl1), pp.S44-S63.

[3] Folkes, V.S., 1982. Forming relationships and the matching hypothesis. *Personality and Social Psychology Bulletin*, 8(4), pp.631-636.

[4] Schmidt, R.C. and Fitzpatrick, P.A., 2014, October. Understanding the motor dynamics of interpersonal interactions. In SMC (pp. 760-764).

[5] Walton, A.E., Richardson, M.J., Langland-Hassan, P. and Chemero, A., 2015. Improvisation and the self-organization of multiple musical bodies. *Frontiers in psychology*, 6, p.313.

[6] Wiltermuth, S.S. and Heath, C., 2009. Synchrony and cooperation. *Psychological science*, 20(1), pp.1-5.

[7] Raffard, S., Salesse, R.N., Marin, L., Del-Monte, J., Schmidt, R.C., Varlet, M., Bardy, B.G., Boulenger, J.P. and Capdevielle, D., 2015. Social priming enhances interpersonal synchronization and feeling of connectedness towards schizophrenia patients. *Scientific reports*, 5, p.8156.

[8] Feniger-Schaal, R., Noy, L., Hart, Y., Koren-Karie, N., Mayo, A.E. and Alon, U., 2016. Would you like to play together? Adults' attachment and the mirror game. *Attachment & human development*, 18(1), pp.33-45.

[9] Noy, L., Dekel, E. and Alon, U., 2011. The mirror game as a paradigm for studying the dynamics of two people improvising motion together. *Proceedings of the National Academy of Sciences*, 108(52), pp.20947-20952.

[10] Noy, L., Levit-Binun, N. and Golland, Y., 2015. Being in the zone: physiological markers of togetherness in joint improvisation. *Frontiers in human neuroscience*, 9, p.187.

[11] Zhai, C., Alderisio, F., Tsaneva-Atanasova, K. and Di Bernardo, M., 2014, October. A novel cognitive architecture for a human-like virtual player in the mirror game. In Systems, Man and Cybernetics (SMC), 2014 IEEE International Conference on (pp. 754-759). IEEE.

[12] http://www.euromov.eu/alterego/.

[13] Sharifi, M., Behzadipour, S. and Vossoughi, G., 2014. Nonlinear model reference adaptive impedance control for human-robot interactions. *Control Engineering Practice*, 32, pp.9-27.

[14] Liu, Y. and Zhang, Y., 2014. Control of human arm movement in machine-human cooperative welding process. *Control Engineering Practice*, 32, pp.161-171.

[15] Boucenna, S., Cohen, D., Meltzoff, A.N., Gaussier, P. and Chetouani, M., 2016. Robots learn to recognize individuals from imitative encounters with people and avatars. *Scientific reports*, 6, p.19908.

[16] Boucenna, S., Anzalone, S., Tilmont, E., Cohen, D. and Chetouani, M., 2014. Learning of social signatures through imitation game between a robot and a human partner. *IEEE Transactions on Autonomous Mental Development*, 6(3), pp.213-225.

[17] Słowiński, P., Zhai, C., Alderisio, F., Salesse, R., Gueugnon, M., Marin, L., Bardy, B.G., Di Bernardo, M. and Tsaneva-Atanasova, K., 2016. Dynamic similarity promotes interpersonal coordination in joint action. *Journal of The Royal Society Interface*, 13(116), p.20151093.

[18] Hart, Y., Noy, L., Feniger-Schaal, R., Mayo, A.E. and Alon, U., 2014. Individuality and togetherness in joint improvised motion. *PloS one*, 9(2), p.e87213.

[19] Zhai, C., Alderisio, F., Tsaneva-Atanasova, K. and Di Bernardo, M., 2015, December. A model predictive approach to control the motion of a virtual player in the mirror game. In *Decision and Control (CDC), 2015 IEEE 54th Annual Conference on* (pp. 3175-3180). IEEE.

[20] Zhai, C., Alderisio, F., Słowiński, P., Tsaneva-Atanasova, K. and di Bernardo, M., 2016. Design of a virtual player for joint improvisation with humans in the mirror game. *PloS one*, 11(4), p.e0154361.

[21] Mörtl, A., Lorenz, T. and Hirche, S., 2014. Rhythm patterns interaction-synchronization behavior for human-robot joint action. *PloS one*, 9(4), p.e95195.

[22] Dumas, G., de Guzman, G.C., Tognoli, E. and Kelso, J.S., 2014. The human dynamic clamp as a paradigm for social interaction. *Proceedings of the National Academy of Sciences*, 111(35), pp.E3726-E3734.

[23] Zhai, C., Alderisio, F., Tsaneva-Atanasova, K. and Di Bernardo, M., 2014, December. Adaptive tracking control of a virtual player in the mirror game. In Decision and Control (CDC), 2014 IEEE 53rd Annual Conference on (pp. 7005-7010). IEEE.

[24] Kelso, J.S., de Guzman, G.C., Reveley, C. and Tognoli, E., 2009. Virtual partner interaction (VPI): exploring novel behaviors via coordination dynamics. *PloS one*, 4(6), p.e5749.

[25] Haken, H., Kelso, J.S. and Bunz, H., 1985. A theoretical model of phase transitions in human hand movements. *Biological cybernetics*, 51(5), pp.347-356.

[26] Zhai, C., Alderisio, F., Słowiński, P., Tsaneva-Atanasova, K. and di Bernardo, M., 2018. Design and validation of a virtual player for studying interpersonal coordination in the mirror game. *IEEE transactions on cybernetics*, 48(3), pp.1018-1029.

[27] Dahan, A., Noy, L., Hart, Y., Mayo, A. and Alon, U., 2016. Exit from synchrony in joint improvised motion. *PloS one*, 11(10), p.e0160747.

[28] Słowiński, P., Rooke, E., Di Bernardo, M. and Tanaseva-Atanasova, K., 2014. Kinematic characteristics of motion in the mirror game. Institute of Electrical and Electronics Engineers.

[29] Słowiński, P., Alderisio, F., Zhai, C., Shen, Y., Tino, P., Bortolon, C., Capdevielle, D., Cohen, L., Khoramshahi, M., Billard, A. and Salesse, R., 2017. Unravelling socio-motor biomarkers in schizophrenia. *npj Schizophrenia*, 3(1), p.8.

[30] Flash, T. and Hogan, N., 1985. The coordination of arm movements: an experimentally confirmed mathematical model. *Journal of neuroscience*, 5(7), pp.1688-1703.

[31] Kalinina, E.A. and Uteshev, A.Y., 2002. Elimination theory. St. Petersburg State University.

[32] Alderisio, F., Antonacci, D., Zhai, C. and di Bernardo, M., 2016, June. Comparing different control approaches to implement a human-like virtual player in the mirror game. In Control Conference (ECC), 2016 European (pp. 216-221). IEEE.

[33] Kreuz, T., Mormann, F., Andrzejak, R.G., Kraskov, A., Lehnertz, K. and Grassberger, P., 2007. Measuring synchronization in coupled model systems: A comparison of different approaches. *Physica D: Nonlinear Phenomena*, 225(1), pp.29-42.

[34] Alderisio, F., Lombardi, M., Fiore, G. and di Bernardo, M., 2017. A novel computer-based set-up to study movement coordination in human ensembles. *Frontiers in psychology*, 8, p.967.

[35] Chen, M.Z., Zhang, L., Su, H. and Chen, G., 2016. Stabilizing solution and parameter dependence of modified algebraic Riccati equation with application to discrete-time network synchronization. *IEEE Transactions on Automatic Control*, 61(1), pp.228-233.

[36] Chen, M.Z., Zhang, L., Su, H. and Li, C., 2015. Event-based synchronisation of linear discrete-time dynamical networks. *IET Control Theory & Applications*, 9(5), pp.755-765.

[37] Alderisio, F., Fiore, G., Salesse, R.N., Bardy, B.G. and Di Bernardo, M., 2017. Interaction patterns and individual dynamics shape the way we move in synchrony. *Scientific reports*, 7(1), p.6846.

[38] Alderisio, F., Bardy, B.G. and Di Bernardo, M., 2016. Entrainment and synchronization in networks of RayleighCvan der Pol oscillators with diffusive and Haken-Kelso-Bunz couplings. *Biological cybernetics*, 110(2-3), pp.151-169.